High speed VNIR/SWIR HSI sensor for vegetation trait mapping

Julia R. Dupuis*, S. Chase Buchanan, Stephanie Craig, J. D. Rameau, and David Mansur

Physical Science Inc., 20 New England Business Center, Andover, MA 01810
Tel: 978-689-0003; Fax: 978-689-3232; *jdupuis@psicorp.com; www.psicorp.com

ABSTRACT

A high-speed visible/near infrared, shortwave infrared (VNIR/SWIR) hyperspectral imaging (HSI) sensor for airborne, dynamic, spatially-resolved vegetation trait measurements in support of advanced terrestrial modeling is presented. The VNIR/SWIR-HSI sensor employs a digital micromirror device as an agile, programmable entrance slit into VNIR (0.5–1μm) and SWIR (1.2–2.4μm) grating spectrometer channels, each with a two-dimensional focal plane array. The sensor architecture, realized in a 13 lb package, is specifically tailored for deployment on a small rotary wing (hovering) unmanned aircraft system (UAS). The architecture breaks the interdependency between aircraft speed, frame rate, and spatial resolution characteristic of push-broom HSI systems. The approach enables imaging while hovering as well as flexible revisit and/or foveation over a region of interest without requiring cooperation by the UAS. Hyperspectral data cubes are acquired on the second timescale which alleviates the position accuracy requirements on the UAS's GPS-IMU. The sensor employs a simultaneous and boresighted visible context imager for pan sharpening and orthorectification. The data product is a 384×290 (spatial) ×340 (spectral) format calibrated, orthorectified spectral reflectivity data cube with a 26×20° field of view.

The development, characterization, and a series of capability demonstrations of an advanced prototype VNIR/SWIR HSI sensor are presented. Capability demonstrations include ground-based testing as well as flight testing from a commercial rotary wing UAS with remote operation of the HSI sensor via a dedicated ground station.

Key Words: visible-near infrared, shortwave infrared, hyperspectral imaging sensor, digital micromirror device, vegetation trait mapping, unmanned aircraft system

1. TECHNOLOGY OVERVIEW

Physical Sciences Inc. (PSI) developed a high-speed visible/near infrared, shortwave infrared (VNIR/SWIR) hyperspectral imaging (HSI) sensor for airborne, dynamic, spatially-resolved vegetation trait measurements to support advanced terrestrial modeling. The VNIR/SWIR-HSI sensor employs a digital micromirror device (DMD) as an agile, programmable entrance slit into VNIR and SWIR grating spectrometer channels, each with two-dimensional focal plane arrays (FPAs). The DMD-based slit enables the generation of high quality hyperspectral images from a small rotary wing UAS with negligible motion-induced artifacts, setting PSI's technology apart from conventional pushbroom HSI sensors on the market. Figure 1 shows the prototype integrated to a FreeFly Alta8 rotary wing UAS, which was used for airborne testing under this effort.

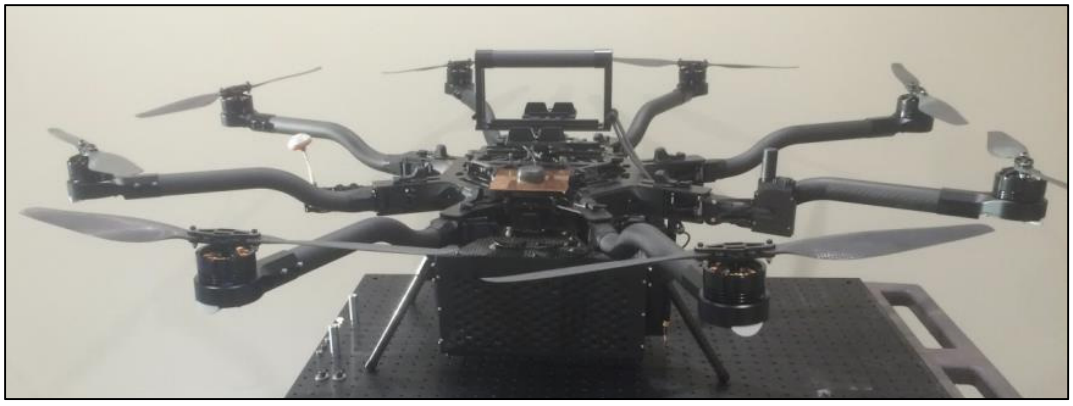

Figure 1: VNIR/SWIR HSI integrated to FreeFly Alta 8 commerical rotary wing UAS.

The key attributes of this technology, shown conceptually in Figure 2, include:

- The DMD-based dynamic spectrometer slit that breaks the interdependency between aircraft speed, frame rate, and spatial resolution of push-broom HSI systems, enabling flexible revisit and/or foveation over an ROI without requiring cooperation by the UAS,
- An extremely compact design containing no macro-moving parts, and
- High speed hyperspectral data acquisition that alleviates the position accuracy requirements on the UAS's GPS-IMU.

The HSI forms an image of the field of view (FOV) onto the DMD which functions as an agile, programmable slit into a dual band grating spectrometer employing CMOS and SWIR mercury cadmium telluride (MCT) FPAs. The FPAs detect the +1st diffracted order from the slit, thereby simultaneously capturing spectral information, corresponding to each spatial resolution element coincident with the slit, every frame. The DMD scans the slit over the image, and frames are synchronously acquired to build up the hyperspectral cube. Because the slit is electro-optically scanned, the system does not require motion by the aircraft and has no inherent interdependence between spatial resolution, frame rate, and aircraft velocity. Hyperspectral cubes are formed post process by reordering the columns, which is a computationally simple process. The sensor includes a simultaneous and boresighted visible context imager which is used for orthorectification post process (not covered in this paper).

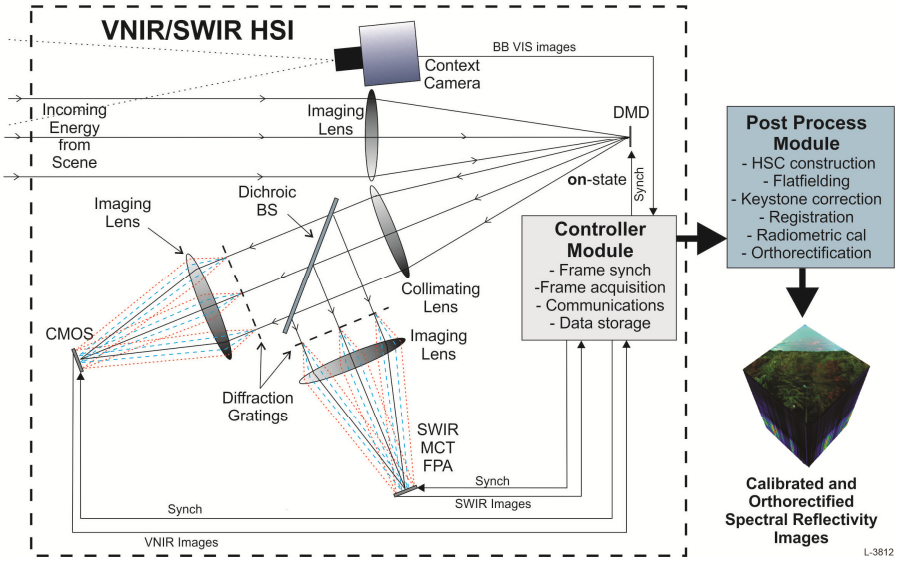

Figure 2: Schematic showing the VNIR/SWIR system concept.

Capability specific key performance parameters (KPPs) for the VNIR/SWIR HSI sensor are listed in Table 1. The UAS maximum altitude falls below that regulated by the FAA and is anticipated for most deployment. UAS velocity spans a stationary multirotor UAS to a small fixed wing UAS. The spectral range spans typically exploited vegetation reflection features [1]. The spectral resolution and minimum spectral reflectivity modulation requirements are sufficient to spectrally and radiometrically resolve typical vegetation features, respectively. Size, weight, and power (SWaP) are specified to meet small (Threshold) and micro (Objective) UAS maximum payloads.

Table 1: System Key Performance Parameters

Parameter	Threshold [Objective]
Ground Sample Distance (GSD)	≤ 30 cm
FOV	≥ 30º
UAS maximum altitude	≤ 400 ft
UAS velocity	Hovering to 25 m/s
Spectral range	0.5 – 2.4 µm [0.35 – 2.5 µm]
Spectral resolution	10 nm
Minimum detectable spectral refl. modulation	2% [1%]
Wavelength accuracy	± 1 nm
Operation time	30 min [60 min]
Size	10,000 cm^3 [5000 cm^3]
Weight	10 kg [5 kg]
Power	Self-powered

2. DESIGN SUMMARY

Figure 3 shows the full optical layout including fore optics which form an image of the field onto the DMD, a total internal reflection (TIR) prism which separates ingoing and outgoing light to/from the DMD by angle, a collimating lens and dichroic beamsplitter, and SWIR and VNIR gratings and imaging optics which form an image of the dispersed slit onto their respective FPAs. The fore optics are telecentric and accommodate a 30° FOV onto the DMD. VNIR and SWIR optical trains were designed to maintain a modulation transfer function greater than 10% over the full FOV and respective spectral range at the relevant spatial frequency associated with a single spatial/spectral resolution element. This performance insures compliance with GSD and spectral resolution KPPs listed in Table 1. The right panel of Figure 3 shows (Zemax) footprint diagrams of the VNIR (upper) and SWIR (lower) channels showing the requisite dispersion of 242 pixels by the respective spectral ranges. These diagrams show that the system achieves the requisite magnification of the DMD onto each FPA with the correct dispersion to meet spectral range and resolution KPPs.

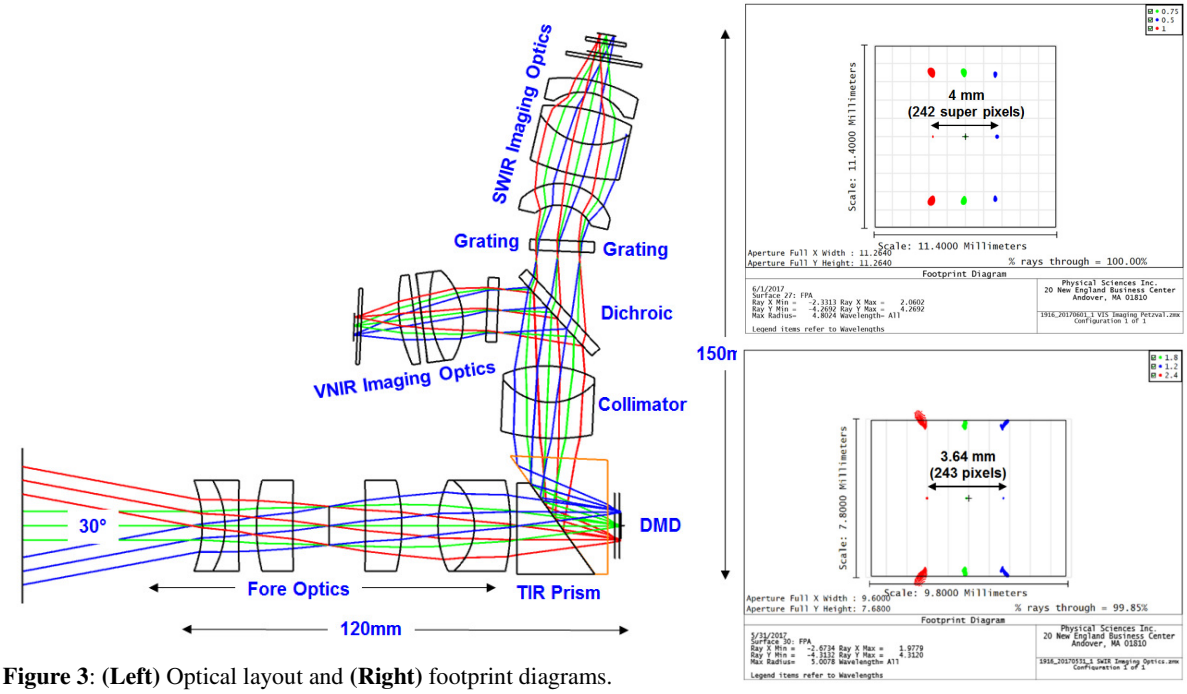

Figure 3: **(Left)** Optical layout and **(Right)** footprint diagrams.

Figure 4 shows the full mechanical package assembly as flown. The dimensions are 12×10×4.5-inches, and the cover is thin sheet metal. In flight, the system looks down through a viewing port window on the undersurface of the package. The fold mirror points the FOV through the fore optics and onto the DMD as shown. The sensor was built and aligned with the ground facing surface up where all subassemblies mount to a light-weighted baseplate which mounts to the top of the box in operation. Two cube assemblies function as opto-mechanical interfaces: the TIR prism cube interfaces the fore optics with the DMD and collimating lens shown in Figure 3, and the dichroic beamsplitter/grating cube

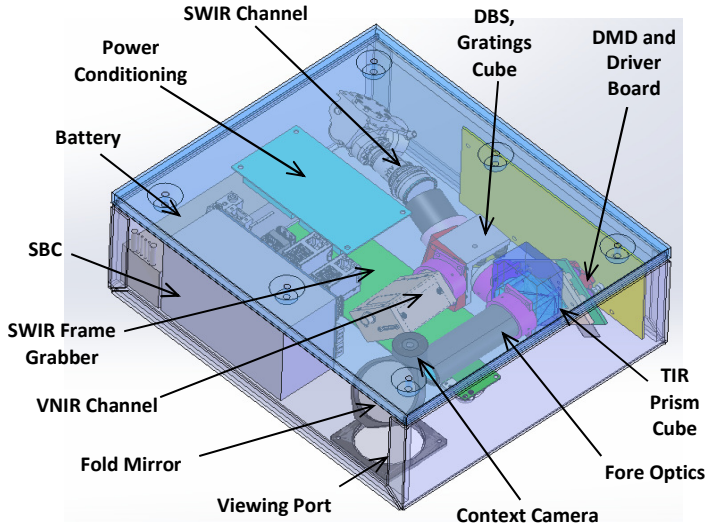

Figure 4: HSI package as flown (down looking).

interfaces with the SWIR and VNIR imaging channels.

The custom ground control station (GCS) is shown in Figure 5a and provides remote control for operations, Ethernet and Wi-Fi for ground connection between a Toughbook laptop hosting the User Interface (UI) and the tripod-mounted or UAS deployed HSI. The GCS can run on shore power indefinitely or on batteries for more than 2 hours. A Raspberry Pi functions as a proxy to communications for wireless operation from the Toughbook. The enclosure and all external connections are water resistant and ruggedized for outdoor operation. Figure 5b is a screen shot of the UI on the Toughbook. The UI includes a waypoint planning capability, heading information, and all requisite HSI controls.

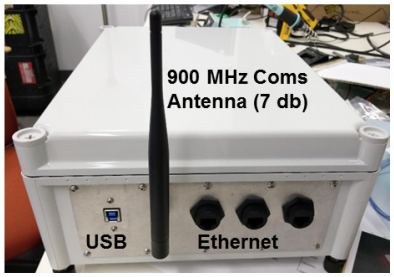

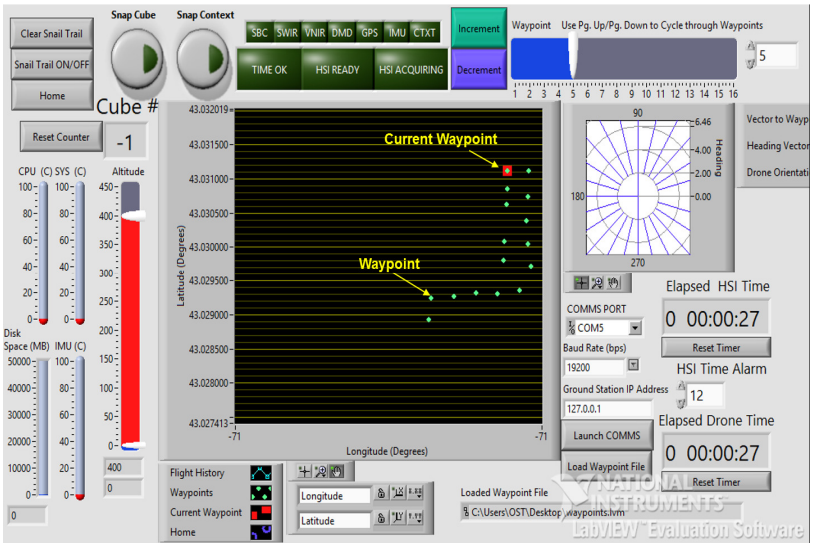

Figure 5: (Left) GCS photo **(Right)** UI

3. Functional Testing

Figure 6 shows the predicted spatially resolved signal to noise ratio (SNR) as a function of wavelength based on readout and shot noise sources in each channel in concert with the per-spectral/spatial resolution element throughput and surface losses. The model assumes clear sky illumination and a 100% diffuse reflecting target (e.g. Spectralon). The model supports an ability to resolve a 0.5% reflectivity modulation in the VNIR and a 1% reflectivity modulation in the SWIR for a 100% diffuse reflective target. These resolution values are generally maintained or improved with reduced target reflectivity owing to the dominant shot noise limit. In other words, a 2× target reflectivity reduction reduces the requisite SNR to maintain a given reflectivity resolution by 2×, but reduces the actual SNR by only √2. SNR values were validated in the lab using the visible and SWIR lasers discussed below to illuminate a roughened aluminum target with near-solar spectral irradiance and measuring sensor noise in time.

Figure 7 shows measured spectral resolution data for VNIR and SWIR channels. For this data set, 532 and 1550 nm lasers were used to illuminate a roughened aluminum target board at various points in the field, and the full width at half maximum (FWHM) of the spatially resolved spectra was quantified based on a Gaussian fit. Figure 7a shows the VNIR response of one pixel near the center of the FOV with a FWHM of 3.7 nm, which exceeds the 10 nm requirement and agrees well with the theoretical limit of 4 nm. Figure 7b shows the SWIR response of the same pixel near the center of the FOV with a FWHM of 13.8 nm which falls short of the 10 nm requirement but is more than sufficient for spectral discrimination in the intended application. Of note is that this data was acquired

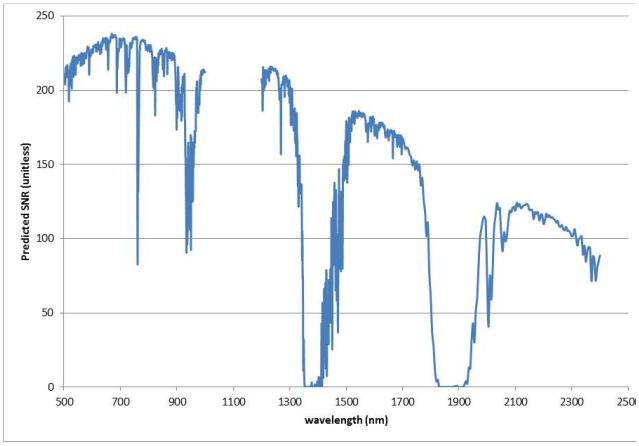

Figure 6: Predicted SNR spectrum.

and processed prior to a final wavelength calibration and the exact wavelength values are off. Also of note are the very low background levels indicating good out-of-band rejection. The DMD-based slit enables in situ background/stray light measurement and subtraction from subsequent frames, which effectively nulls these effects.

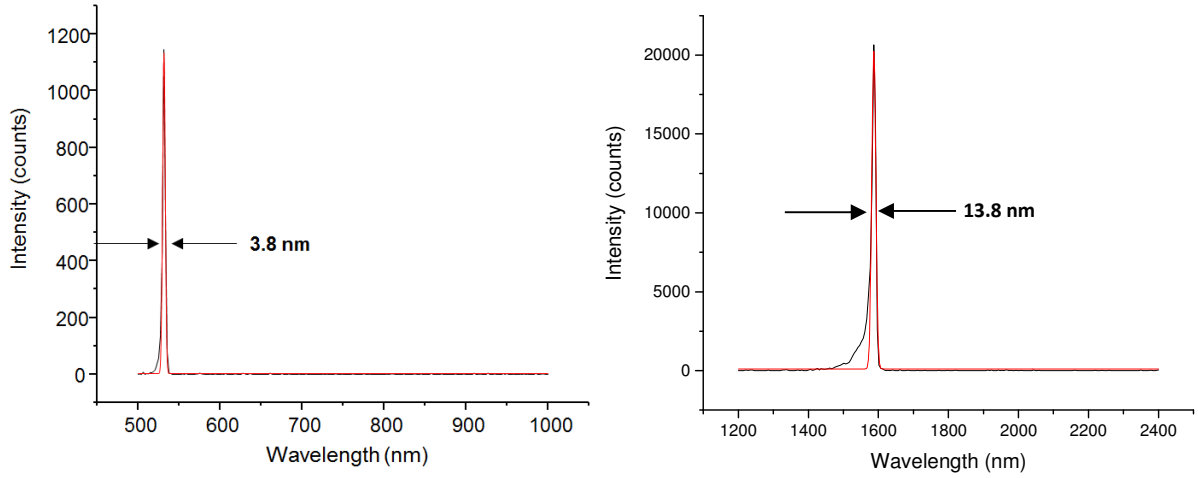

Figure 7: (Left) VNIR spectral resolution data: spectral response of one pixel near the center of the FOV to a 532 nm laser. **(Right)** SWIR spectral resolution data: spectral response of one pixel near the center of the FOV to a 1550 nm laser.

4. DEVELOPMENTAL TESTING

Ground based field testing was performed locally in Andover, MA and in Epping, NH where PSI has an off-site location for field testing. For all of the ground tests the HSI was mounted on a tripod and used to acquire data of grass and trees in the far field.

4.1 Ground Based Testing

Figure 8 shows VNIR and SWIR images acquired with the HSI mounted on the tripod at the Epping site. The spectral images were flat fielded and calibrated to produce spectral reflectivity data, and the resulting data cubes were then average over the two spectral channels for display purposes only shown in Figure 8. Note that calibration is relative to the flat fielding illumination conditions and can result in > 1 reflectivity. Figure 8 shows ROIs compared in VNIR and SWIR channels containing live trees (black boxes) and dead dry grass (red boxes). Figure 9 shows the corresponding spectra (5×5 pixel binned) above literature spectra of live and dead vegetation. The data shows the expected reflectivity differences in VNIR and SWIR channels. The live tree spectral shows the expected 550 nm green peak, and the dry grass shows higher reflectivity in the SWIR spectral range due to lower water content.

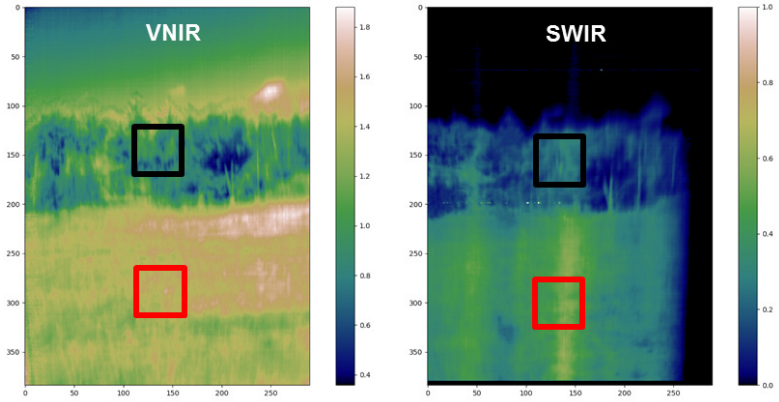

Figure 8: (Left) VNIR and **(Right)** SWIR summed images with live (black) and dead (red) vegetation ROIs.

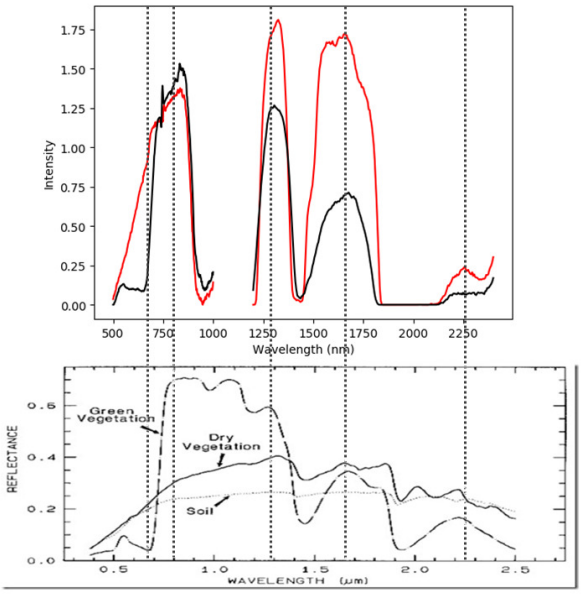

Figure 9: (Top) Dead (red) and live (black) vegetation spectra acquired with HSI corresponding to boxes in Figure 8. **(Bottom)** corresponding literature spectra showing same features.

The next set of figures compare HSI data of live and dead grass acquired at one of the performer's lawns and at Epping respectively. The stacked images are shown in the left two columns of Figure 10 and corresponding spectra are shown in the right column. Again, the expected differences between live and dead vegetation are present.

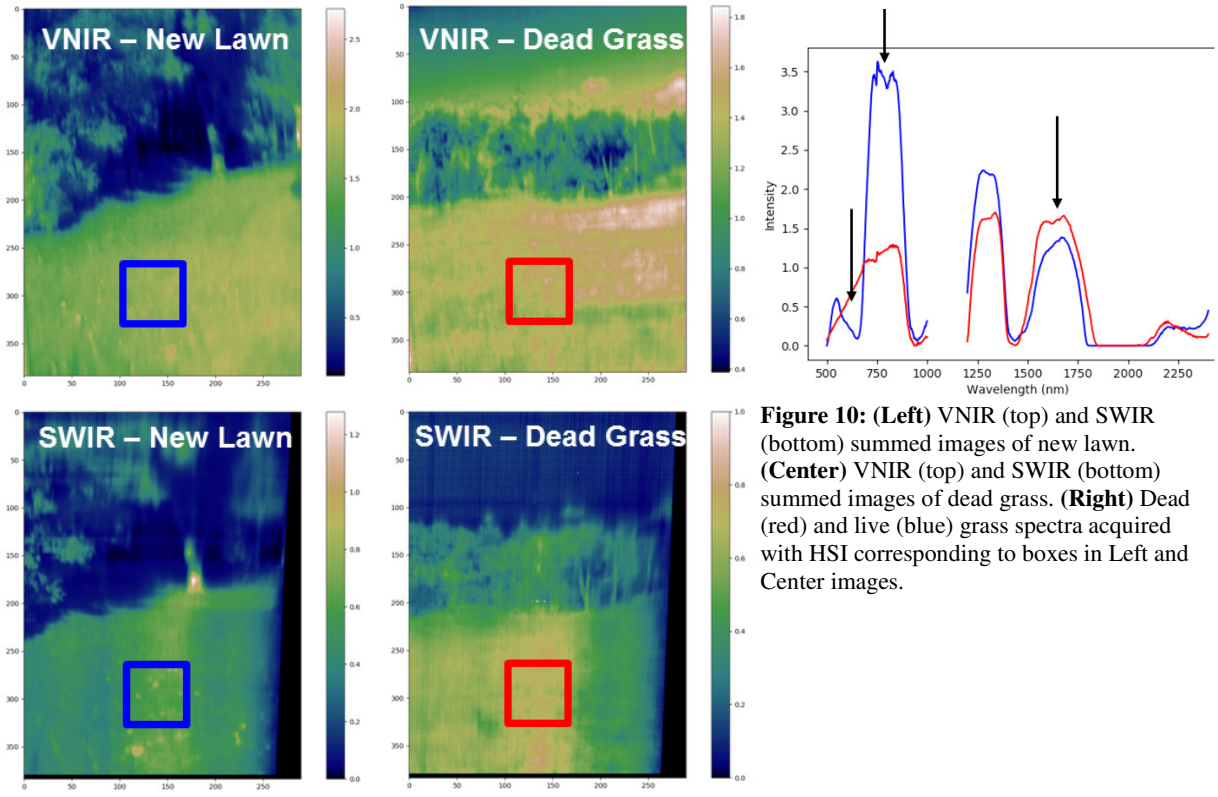

Figure 10: (Left) VNIR (top) and SWIR (bottom) summed images of new lawn. **(Center)** VNIR (top) and SWIR (bottom) summed images of dead grass. **(Right)** Dead (red) and live (blue) grass spectra acquired with HSI corresponding to boxes in Left and Center images.

4.2 Airborne Testing

Figure 11 shows the set up for flight testing at the Epping, NH location. The HSI is connected to the Alta8 using the toad-in-the-hole mount. The operating procedure was to initialize the sensor, GPS, communications, and UI while connected to shore power to preserve the HSI's batteries, particularly until the SWIR FPA has throttled. Once, initialized, the sensor was switched to battery power immediately before takeoff.

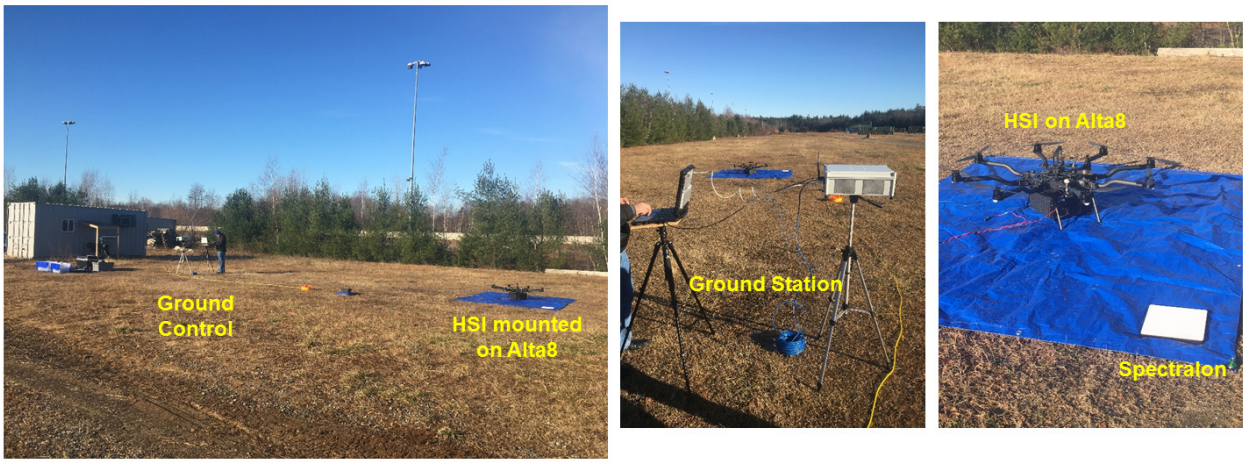

Figure 11: Set up for flight testing at Epping, NH location.

In-flight spectro-radiometric calibration makes use of an image of the Spectralon target located on the tarp to capture the intensity of the sunlight that day and at that time. The measured solar spectrum is later used to convert the rest of the data cube to absolute spectral reflectivity units. Figure 12 shows images of the Spectralon target acquired at 100 feet (left), 250 feet (center) and 400 feet (right) on a low sunlight day. The Spectralon piece is approximately 30 cm (i.e. same size as the GSD). The Spectralon is just discernible in the 400 foot image confirming achievement of the GSD and maximum altitude KPPs.

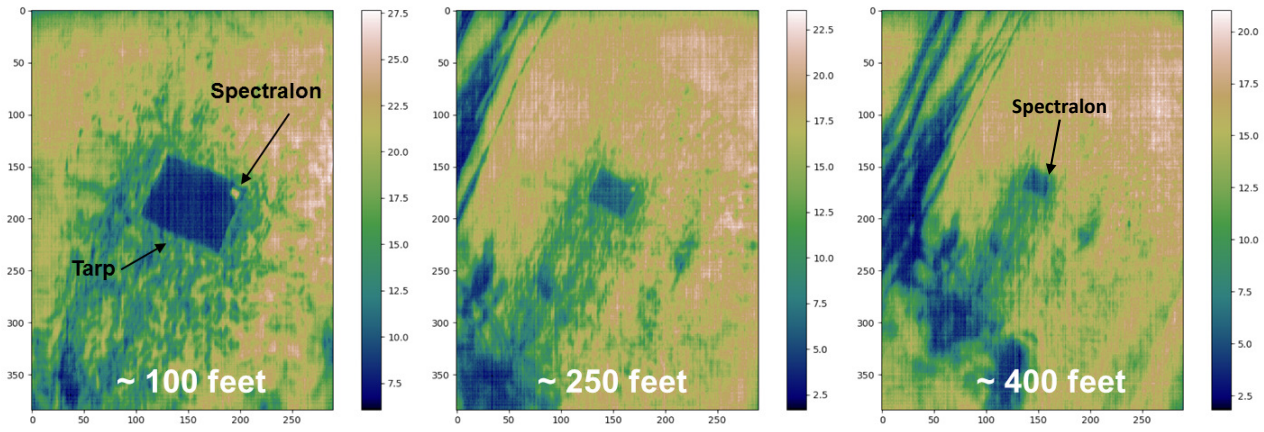

Figure 12: Spectrally summed image of tarp and Spectralon at 100 feet (left), 250 feet (center) and 400 feet (right) UAS altitude.

Figure 13 shows VNIR and SWIR summed images acquired over trees from the Alta8. Spectra from the corresponding ROIs are shown on the right where the red box contains dead vegetation and the blue live. As before, the dead vegetation appears brighter in the SWIR than the VNIR owing to the decreased water content (increased SWIR reflectivity). The live vegetation appears brighter overall, although this is partially due to the flat fielding of these particular images. The water feature at 750 nm was more pronounced in all airborne data because of the significant path through the atmosphere relative to the flat field condition.

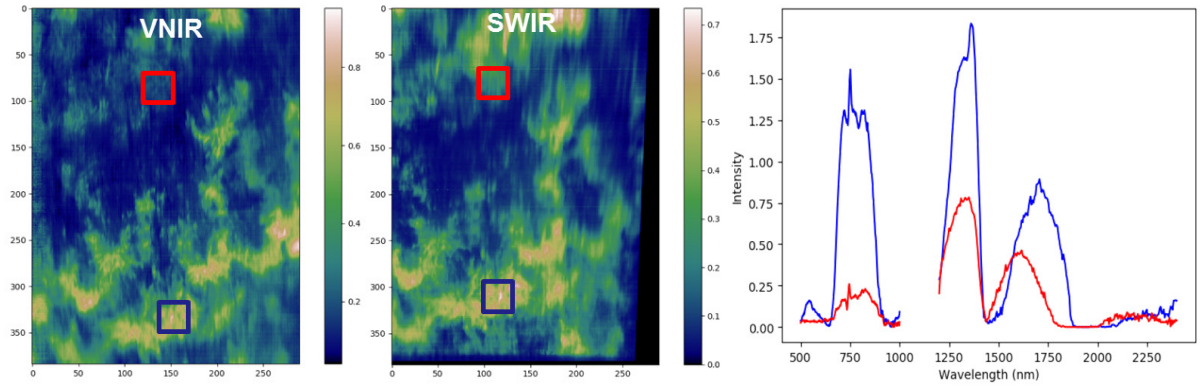

Figure 13: (Left) VNIR and **(Center)** SWIR summed images acquired from airborne HSI over trees. Boxed areas indicate dead (red) and live (blue) vegetation. **(Right)** Live (blue) and dead (red) vegetation spectra corresponding to ROIs.

A spectral angle mapping (SAM) algorithm was applied to the over-tree data shown in Figure 13. The result is shown in Figure 14 where red indicates high SAM value for dead vegetation, cyan indicates high SAM value for live vegetation, and purple is not a good match to either. Figure 14 is effectively a vegetation map which is the intended ultimate product of this project.

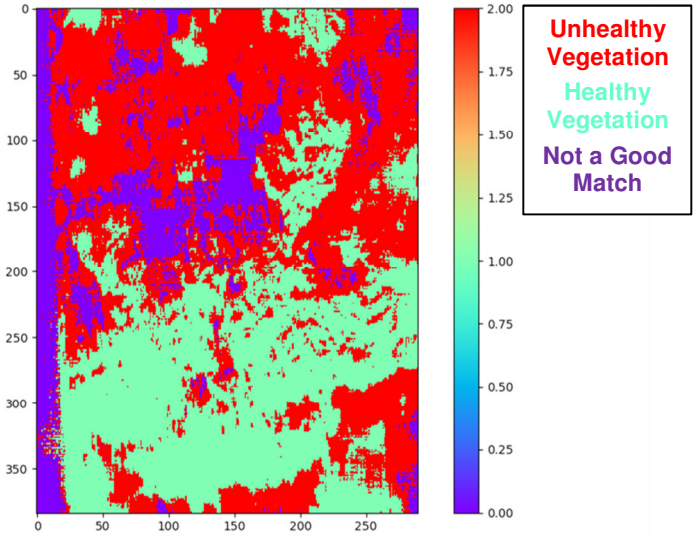

Figure 14: SAM map showing regiong of dead (red) and healthy (cyan) vegetation. Purple indicates a lower SAM value (matches neither).

The next airborne data set was acquired over the dragway at Epping and includes trees, dirt and pavement. The context camera was overexposed for all of these data sets, and the image is therefore not presented. Instead a Google image is included based on the GPS coordinates that matches well with the observed VNIR and SWIR images shown in Figure 15. Of particular note is the image quality in VNIR and SWIR summed images which have undergone no motion stability correction. The light post shadow is very well resolved, as are the structures in the tree shadows. Figure 15 shows spectra from the three ROIs indicated in the left side images containing concrete (black), dead grass (blue) and a conifer bush (green) along with literature spectra. The measured spectra generally agree with the expected spectral shapes.

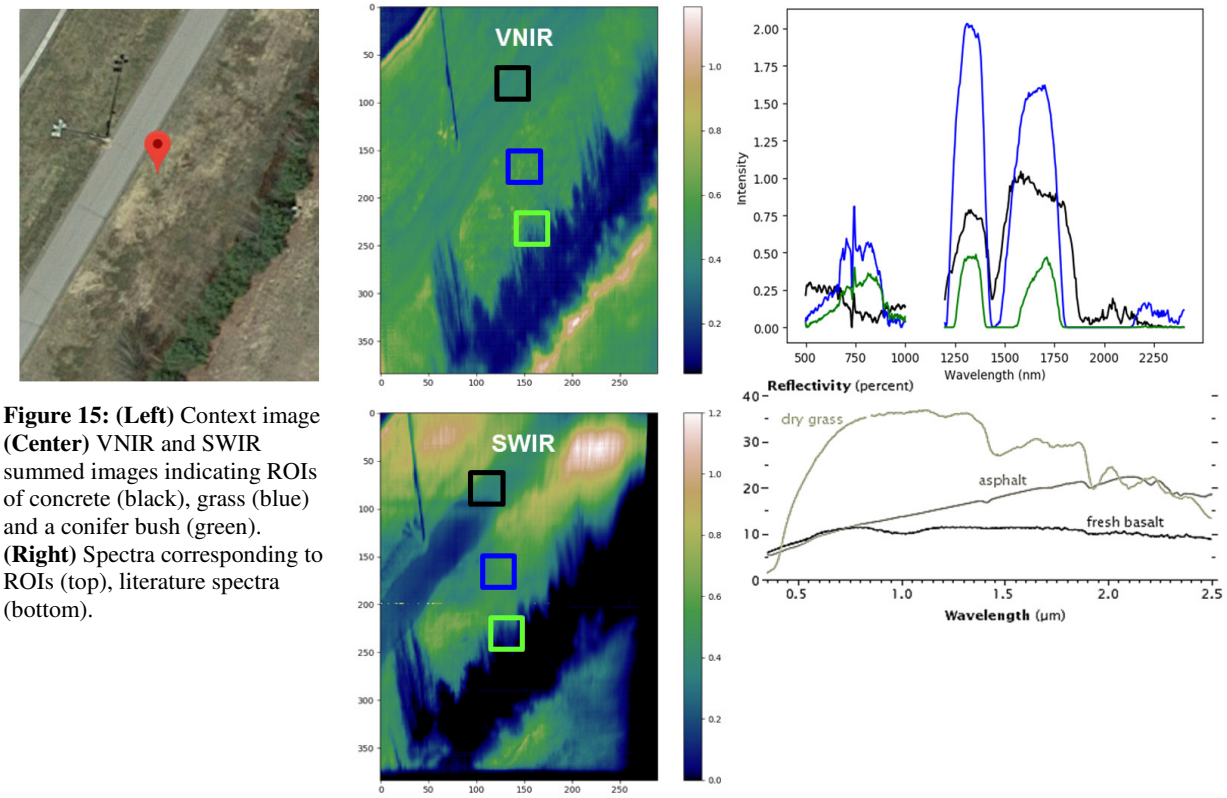

Figure 15: (Left) Context image **(Center)** VNIR and SWIR summed images indicating ROIs of concrete (black), grass (blue) and a conifer bush (green). **(Right)** Spectra corresponding to ROIs (top), literature spectra (bottom).

4.3 Capability Demonstration: Disturbed Earth Detection

The next data series show the results of a capability demonstration for the detection of disturbed earth with application to landmine and improvised explosives device (IED) detection. The initial demonstration had the HSI tripod mounted and acquiring hyperspectral data before and after a series of holes were dug up and the dirt turned over in the field at the Epping, NH location. Figure 16 shows spectrally summed VNIR (upper) and SWIR (lower) images after digging (left column) and the difference between before and after (left center column). The bright spikes are wooden hole-markers. The four boxes on the right show spectra corresponding to the four ROIs before (blue trace) and after (red trace) digging. The relevant phenomenology is a reflectivity depression in the SWIR owing to increased moisture in the upturned soils (absorbs more SWIR light). In general the reflectivity in the VNIR is about the same before and after (i.e. the holes are not detectable by eye).

Figure 17 shows the result of a SAM map applied to match disturbed earth spectral features across the full FOV. All holes were properly identified, and most of the matches in the near field are the experimentalists' footprints. Morphological filters were used in the next series of (airborne) tests to further control false positives (and reject footprints). However, the basic capability was demonstrated with these ground based measurements.

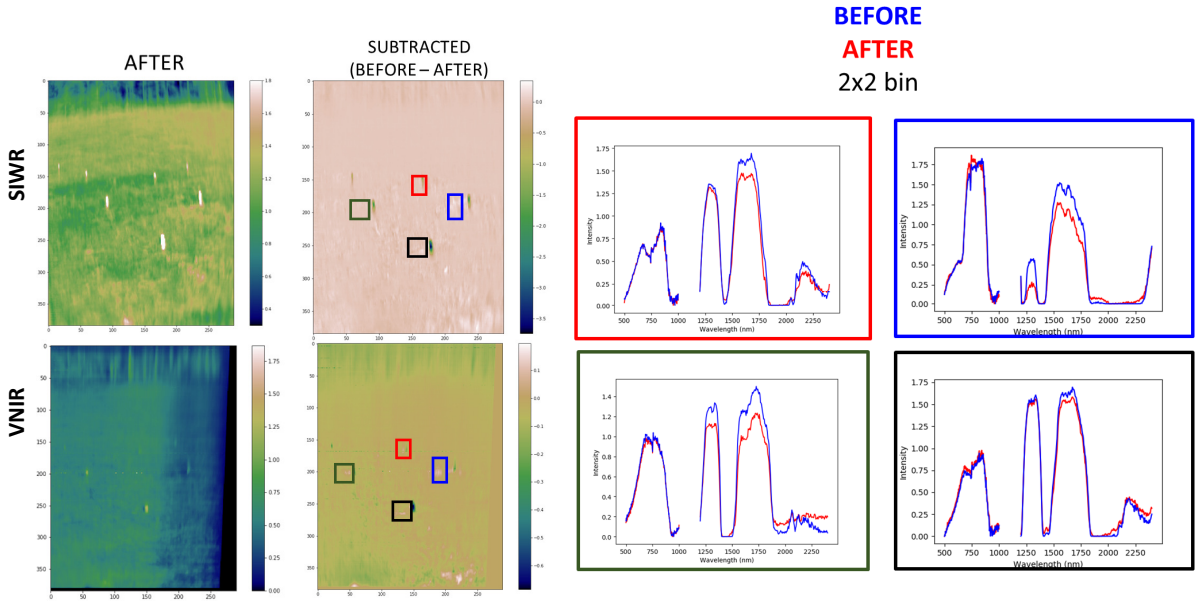

Figure 16: (Left) VNIR (upper) and SWIR (lower) spectrally summed images of disturbed earth. **(Center)** Difference images between before and after earth was disturbed. **(Right)** Before and after spectra from four ROIs showing depressed reflectivity in the SWIR due to upturned moisture.

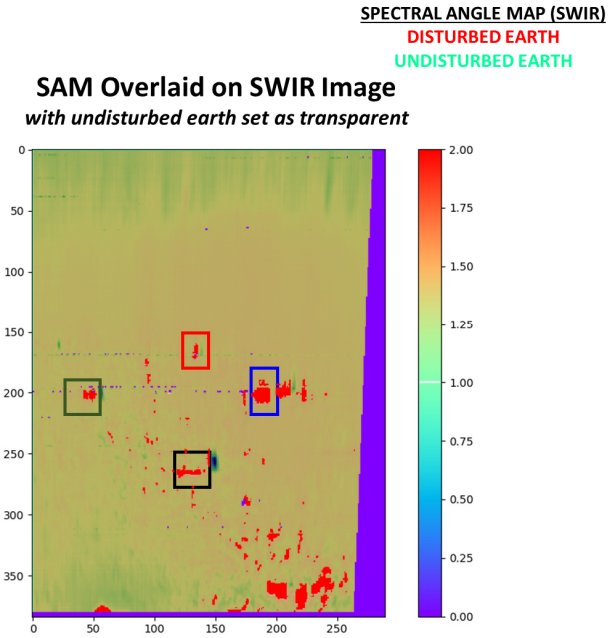

Figure 17: SAM detection map for disturbed earth.

The next capability demonstration was the detection of disturbed earth in a beach zone with application to land and underwater mine detection. These were airborne tests, and unlike the previous demonstration, there is no before and after data to analyze. The analysis is based on local spectral similarities and shape (detailed below). This demonstration was conducted at Wallis Sands Beach in Rye, NH (Figure 18). Two sets of 30 holes were prepared on the beach across the following conditions:

- Dry sand above the high tide mark,

- Damp sand between high and low tide marks, which was covered in water 0.5 to 4 hours prior to data collection, and
- Wet sand below the low tide mark.

Holes were prepared by churning sand (Set 1), and by digging and refilling a 6-inch deep hole (Set 2). All holes were approximately 18-24-inches in diameter. Data was acquired from the UAS at 100 ft. altitude which results in approximately 16×16 pixels on each target.

Figure 18: Beach zone test site.

A preliminary disturbed sand detection algorithm was coded as a custom python routine and used to identify regions of interest. The algorithm performs the following steps.

1. Application of a Gaussian blur to the spectral image
2. Use of local thresholds to find low reflectivity regions of the image
3. Application of a morphological "closing" filter
4. Determination of contour lines around the closed shapes
5. A size filtering step
6. An aspect ratio filtering step

Figure 19 show the resulting detection maps. The top row shows the detection overlays (in white) where the black boxes show the target locations. The bottom row shows the spectrally summed images without the overlay for clarity. Images from left to right span dry sand to near ocean (wet) sand. The algorithm successfully identified all disturbed sand for both churned and filled holes with minimal false positives. While the algorithm is very preliminary, again, the basic capability was clearly shown.

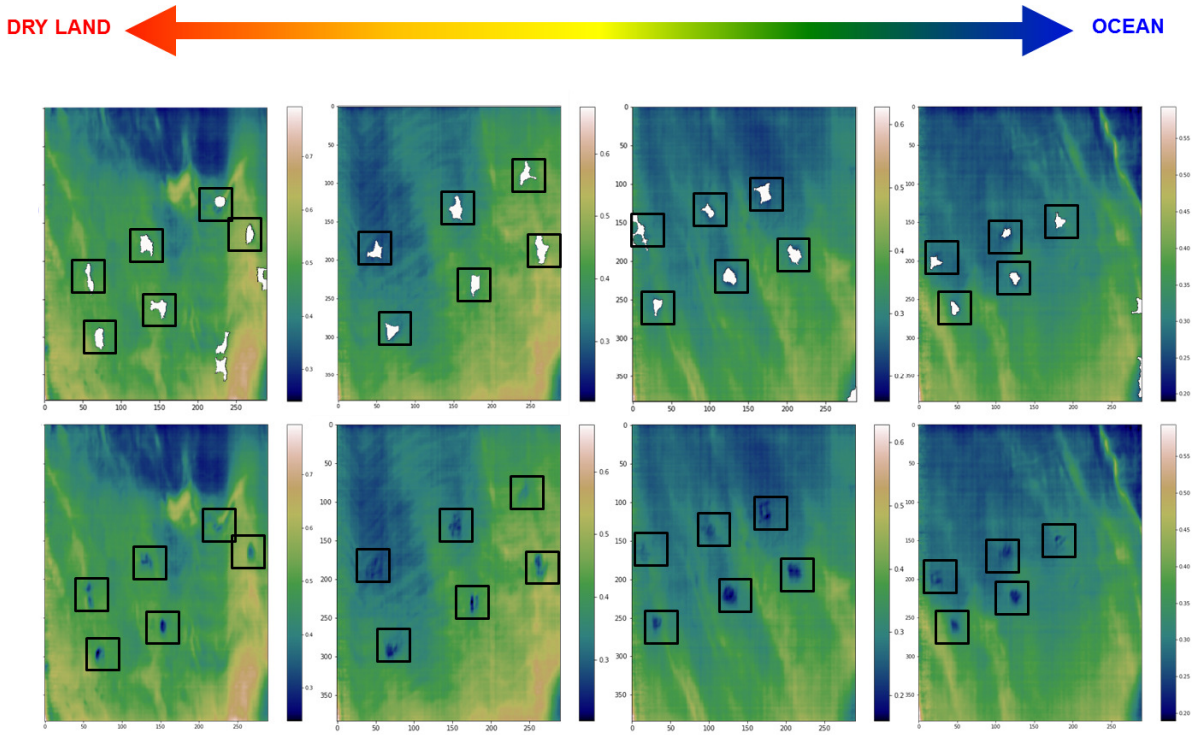

Figure 19: Detection map output overlaid on spectrally summed images (top) and spectrally summed images without overlay (bottom) where boxes indicate ROIs. FOVs are furthest from the water (left) to closest to the water (right).

5. CONCLUSIONS

A high fidelity prototype VNIR/SWIR HSI sensor was designed, built, and validated against the KPPs through functional testing. A custom GCS, communications protocol, and waypoint flight capability were developed for interfacing and flying the HSI on a FreeFly Alta 8 UAS. Calibration, registration, stitching, and orthorectification routines were developed to produce spectral reflectivity maps from the measured raw data. Ground based and airborne developmental testing was conducted, where basic discrimination between surface types, various vegetation, and healthy/unhealthy vegetation was demonstrated. Ground based and airborne capability demonstrations for the detection of disturbed earth and sand were successfully executed. The ability to produce high quality HSI image data from a rotary wing UAS was repeatedly demonstrated, which is a significant attribute of this technology platform.

ACKNOWLEDGEMENTS

This work has been supported by the US Department of Energy, contract no. DE-SC0013149. This support does not constitute an express or implied endorsement on the part of the Government.

REFERENCES

[1] Ustin, Susan L., and John A. Gamon. "Remote sensing of plant functional types." *New Phytologist* 186.4 (2010).